

# Resolving the $H_0$ and $S_8$ tensions with neutrino mass and chemical potential

Shek Yeung,<sup>1,\*</sup> Wangzheng Zhang<sup>1,†</sup> and Ming-chung Chu<sup>1,‡</sup>

<sup>1</sup>*Department of Physics, The Chinese University of Hong Kong, Sha Tin, N.T., Hong Kong*

(Dated: March 19, 2024)

A simple and natural extension of the standard  $\Lambda$ CDM model is to allow relic neutrinos to have non-zero degeneracy. We confront this  $\Lambda$ CDM $\xi$  model,  $\Lambda$ CDM with neutrino mass  $M_\nu$  and degeneracy  $\xi_3$  as additional parameters, with the *Planck* TT, lowT, plik-lensing, BAO, and DES datasets, and we observe a strong preference (Bayes factor  $\log_{10} B = 1.9$ ) for it over the standard  $\Lambda$ CDM model. Both the  $H_0$  and  $S_8$  tensions are resolved to within  $1\sigma$  with the same set of neutrino parameters, along with  $3\sigma$  evidence for nonzero neutrino mass ( $M_\nu = 0.58_{-0.13}^{+0.17}$  eV) and degeneracy ( $\xi_3 = 1.27_{-0.22}^{+0.42}$ ). Furthermore, our analysis favors the scalar index  $n_s$  to be slightly larger than 1, compatible with some hybrid inflation models, as well as a significantly larger optical depth  $\tau$  than the standard Planck value, indicating an earlier onset of reionization.

## INTRODUCTION

The recent availability of high precision cosmological and astrophysical data allows for testing cosmological models in unprecedented details. The Lambda Cold Dark Matter ( $\Lambda$ CDM) model has been very successful in fitting with a wide range of observations [1–10], though there are discordances between different fitting results. The most notable inconsistency is the Hubble tension, a significant discrepancy between the global and local measurements of the Hubble parameter  $H_0$ . Specifically, there is about  $5\sigma$  disagreement between the result obtained by the Planck collaboration [1],  $H_0 = 67.36 \pm 0.54$  km s<sup>-1</sup>Mpc<sup>-1</sup> at a 68% confidence level (CL) derived from the anisotropies of the cosmic microwave background (CMB) TT, TE, EE, lowT, lowE and plik-lensing data, and that of the SH0ES collaboration [8],  $H_0 = 73.04 \pm 1.04$  km s<sup>-1</sup>Mpc<sup>-1</sup> at a 68% CL measured using Type Ia supernovae calibrated by Cepheids.

There is another milder tension on the strength of matter clustering, quantified by the parameter  $S_8 \equiv \sigma_8 \sqrt{\Omega_m/0.3}$ , between the measurements through CMB and weak gravitational lensing and galaxy clustering. Here  $\Omega_m$  represents the matter density and  $\sigma_8$  is the standard deviation of matter density fluctuations at radius  $8 h^{-1}$ Mpc extrapolated to redshift 0 according to linear theory, where  $h$  is the dimensionless Hubble parameter. Specifically, there is an approximate  $3\sigma$  discrepancy between  $S_8 = 0.832 \pm 0.013$  at 68% CL from *Planck* CMB using TT, TE, EE, lowT, lowE and plik-lensing data [1] and  $S_8 = 0.759_{-0.021}^{+0.024}$  from KiDS-1000 weak lensing data [9]. More recently, weak lensing observations from the Hyper Suprime-Cam Subaru Strategic Program (HSC-SSP) indicate a slightly lower tension, ranging from  $2 - 2.5\sigma$  depending on the specific methodologies used [11–15].

These tensions could suggest the presence of unknown systematic errors in the cosmological data and/or the existence of new physics beyond  $\Lambda$ CDM. For the latter, a variety of new physics models have been proposed to alleviate both tensions together, such as interacting dark energy (IDE) [16–19], decaying dark matter (DDM) [20], running vacuum model (RVM) [21], graduated dark energy (gDE) [22, 23],  $f(T)$  gravity [24], among others. More detailed discussions on the subject can be found in [25–28]. Nevertheless, effectively resolving both tensions with the same physics while preserving the successes of  $\Lambda$ CDM remains challenging.

In this letter, we consider the  $\Lambda$ CDM +  $M_\nu$  +  $\xi_i$  ( $\Lambda$ CDM $\xi$ ) model as the minimal extension of the  $\Lambda$ CDM model, with  $M_\nu \equiv \sum_i m_i$  and  $\xi_i \equiv \mu_i/T_\nu$  being the neutrino mass and degeneracy parameters, respectively, where  $m_i$  and  $\mu_i$  denote the mass eigenvalue and chemical potential of the  $i^{\text{th}}$  neutrino mass eigenstate, respectively, and  $T_\nu$  is the relic neutrino temperature. Hereafter, following the convention in [1],  $\Lambda$ CDM means the standard cosmological model with fixing  $M_\nu = 0.06$  eV and  $\xi_i = 0$ . While the electron-type neutrino degeneracy parameter  $\xi_e \ll 1$  is tightly constrained by Big Bang nucleosynthesis (BBN) [29, 30], the possibility of  $\mathcal{O}(1)$  degeneracy parameters for muon-type and tau-type neutrinos,  $\nu_\mu, \nu_\tau$ , remains open. Previous studies [31, 32] have shown that nonzero  $\xi_i$  can help alleviate the  $H_0$  tension. Our key result is shown as the blue contours in Figure 1. By fitting with the *Planck* TT, lowT, plik-lensing [1], Baryonic Acoustic Oscillation (BAO) [33–35] and Dark Energy Survey (DES) [36] data, we can resolve both the  $H_0$  and  $S_8$  tensions with the same set of neutrino parameters using the  $\Lambda$ CDM $\xi$  model. Furthermore, there is a  $3\sigma$  evidence for nonzero neutrino mass ( $M_\nu = 0.58_{-0.13}^{+0.17}$  eV) and degeneracy ( $\xi_3 = 1.27_{-0.22}^{+0.42}$ ). Our mean values for the scalar index  $n_s$  and CMB optical depth  $\tau$  differ significantly from the standard Planck values, which have profound implications for our understanding of the early universe.

\* terryys@gmail.com

† 1155129240@link.cuhk.edu.hk

‡ mcchu@phy.cuhk.edu.hk

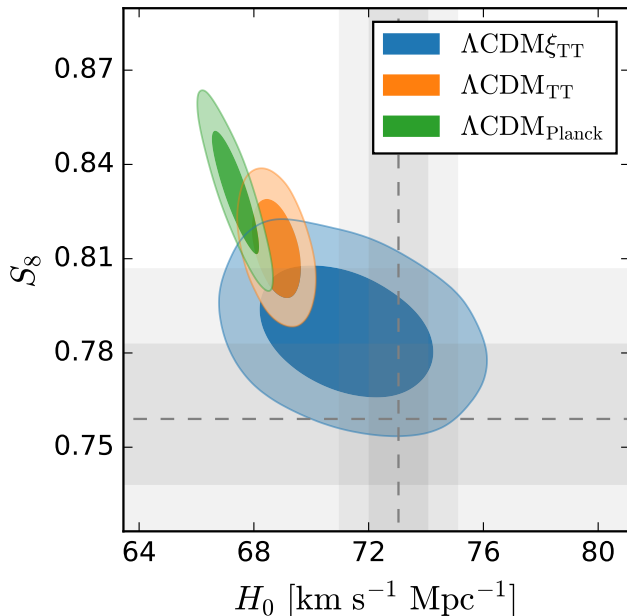


FIG. 1. 2D contours (for 68% CL and 95% CL) for  $H_0$  and  $S_8$ . The Planck results for  $\Lambda$ CDM fitting are denoted as  $\Lambda$ CDM<sub>Planck</sub>, shown as green contours, incorporating *Planck* TT, TE, EE, lowT, lowE and plik–lensing data. The orange and blue contours correspond to the  $\Lambda$ CDM<sub>TT</sub> and  $\Lambda$ CDM $_{\xi_{TT}}$  models, respectively, using *Planck* TT, lowT, plik–lensing, BAO, and DES data. The grey regions represent the 68% and 95% CL for  $H_0$  obtained from SH0ES [8] and for  $S_8$  from KiDS [9], respectively.

## METHODOLOGY

As shown in [37], the neutrino degeneracy becomes diagonal in the mass eigen basis just before neutrino decoupling, and  $\xi_i$  can be related to  $\xi_\alpha$  in the flavor basis by the Pontecorvo–Maki–Nakagawa–Sakata (PMNS) matrix (e.g., Eq. (13) in [37]), where  $\alpha = e, \mu, \tau$ . Based on strong constraints from BBN [29, 30] and the strong mixing between  $\nu_\mu$  and  $\nu_\tau$ , we assume  $\xi_e = 0$  and  $\xi_\mu = \xi_\tau$ . Then we are left with only one free parameter related to neutrino degeneracy, which we choose to be  $\xi_3$ .

The neutrino degeneracy parameters enter the CMB anisotropy calculation through the neutrino energy density,

$$\rho_\nu = \frac{1}{2\pi^2} \sum_{i=1}^3 \int_0^\infty \left[ \frac{\sqrt{p^2 + m_i^2}}{e^{p/T_\nu - \xi_i} + 1} + \frac{\sqrt{p^2 + m_i^2}}{e^{p/T_\nu + \xi_i} + 1} \right] p^2 dp, \quad (1)$$

which plays a role in the expansion history of the universe and the Boltzmann equations. Following [32], we modified CAMB [38, 39] to include these effects in the calculations of the CMB anisotropy power spectra. For more details, please refer to [32]. In this letter, we compare the fitting of cosmological data with two models:  $\Lambda$ CDM model (with  $M_\nu = 0.06$  eV and  $\xi_3 = 0$ ) and

$\Lambda$ CDM $_{\xi}$  model, in which  $M_\nu$  and  $\xi_3$  are allowed to vary.

For the standard Planck data combination, including high-multipole ( $l > 30$ ) *Planck* CMB temperature and polarization anisotropy power spectra (TT, TE, EE) from *Planck* likelihood plik, low-multipole ( $2 \leq l \leq 30$ ) temperature power spectrum (lowT) from Commander, low-multipole ( $2 \leq l \leq 30$ ) polarization power spectrum (lowE) from SimAll and the CMB lensing data (plik–lensing) [1], the results for  $\Lambda$ CDM ( $\Lambda$ CDM<sub>Planck</sub>) are shown as the green contours in Figure 1, which is the standard Planck result [1]. Both  $H_0$  and  $S_8$  are in clear tension with those from SH0ES [8] and KiDS [9], respectively.

The  $\Lambda$ CDM<sub>Planck</sub> constraints on the optical depth  $\tau$  come mainly from the lowE data. However, it is about  $2\sigma$  deviated from that measured by the Atacama Cosmology Telescope (ACT) CMB temperature and polarization combined with BAO data [40]. Also, as discussed in [1], only the CMB temperature spectrum can agree well for two different *Planck* likelihoods plik and CamSpec. Therefore, we will only use the temperature data (TT+lowT) and plik–lensing from CMB. In addition, the neutrino parameters can be better constrained if we include the BAO data from BOSS DR12 “LOWZ” and “CMASS” surveys [35], 6dF Galaxy Survey [33], DR7 Main Galaxy Sample (MGS) [34], and DES data from the Dark Energy Survey [36].

We denote the fitting results of the above data with models  $\Lambda$ CDM and  $\Lambda$ CDM $_{\xi}$  by  $\Lambda$ CDM<sub>TT</sub> and  $\Lambda$ CDM $_{\xi_{TT}}$ , respectively. We use CosmoMC [41, 42] to perform Markov Chain Monte Carlo (MCMC) fitting to get the posterior distributions of the cosmological and neutrino parameters.

## RESULTS

### $H_0$ and $S_8$

Our main results are summarized in Table I. With  $\Lambda$ CDM<sub>TT</sub>, we obtain:

$$\left. \begin{aligned} H_0 &= 68.79 \pm 0.56 \text{ km s}^{-1} \text{ Mpc}^{-1}, \\ S_8 &= 0.813 \pm 0.010. \end{aligned} \right\} 68\% \text{ CL} \quad (2)$$

Moreover, we calculate the deviations (in unit of standard deviations),  $n_\sigma(H_0) = 3.6$  and  $n_\sigma(S_8) = 2.2$ , from the mean values of  $H_0$  and  $S_8$  from the SH0ES ( $H_0 = 73.04 \pm 1.04 \text{ km s}^{-1} \text{ Mpc}^{-1}$ ) [10] and KiDS results ( $S_8 = 0.759^{+0.024}_{-0.021}$ ) [9], respectively, using the Marginalised Posterior Compatibility Level (MPCL) [28], where we treat the latter as Gaussian distributions. We can see that there are still significant tensions in both  $H_0$  and  $S_8$ , only slightly better than those of  $\Lambda$ CDM<sub>Planck</sub>, with  $n_\sigma(H_0) = 4.9$  and  $n_\sigma(S_8) = 2.8$ .

For  $\Lambda\text{CDM}\xi_{\text{TT}}$ , we have

$$\left. \begin{aligned} H_0 &= 71.27_{-2.04}^{+1.97} \text{ km s}^{-1} \text{ Mpc}^{-1}, \\ S_8 &= 0.787 \pm 0.014, \end{aligned} \right\} 68\% \text{ CL} \quad (3)$$

with  $n_\sigma(H_0) = 0.8$  and  $n_\sigma(S_8) = 1.1$ . Both the  $H_0$  and  $S_8$  tensions are resolved with the same set of mean values of  $M_\nu$  and  $\xi_3$ .

We compare the models by the Bayes factor  $B$ :

$$B = \frac{K(\Lambda\text{CDM}_{\text{TT}})}{K(\Lambda\text{CDM}\xi_{\text{TT}})}, \quad (4)$$

where  $K$  is the Bayesian evidence calculated using `MCEvidence` [43]. We obtain  $\log_{10} B = 1.9$ , meaning that the  $\Lambda\text{CDM}\xi$  model is strongly preferred to  $\Lambda\text{CDM}$  by the cosmological data we used. The mean values of all cosmological parameters with 68% CL are summarized in Table II of the Supplemental Materials.

### Other parameters

Figure 2 shows the marginalized posterior 1D PDFs and 2D contours for different cosmological parameters for  $\Lambda\text{CDM}_{\text{Planck}}$  (green),  $\Lambda\text{CDM}_{\text{TT}}$  (orange), and  $\Lambda\text{CDM}\xi_{\text{TT}}$  (blue).

#### neutrino properties: $M_\nu$ and $\xi_3$

For the fitting result of  $\Lambda\text{CDM}\xi_{\text{TT}}$ , we find that cosmological data prefer  $M_\nu = 0.58_{-0.13}^{+0.17}$  eV,  $\xi_3 = 1.27_{-0.22}^{+0.42}$  (68%), with a  $2.8\sigma$  ( $2.9\sigma$ ) evidence for the nonzero  $M_\nu$  ( $\xi_3$ ). The blue contours of Figure 2 show that both the nonzero values of  $M_\nu$  and  $\xi_3$  help to increase  $H_0$  and decrease  $S_8$ .

The sound horizon angular size  $\theta_{\text{MC}} = r_s/D_M$  at photon decoupling ( $z_*$ ) is constrained very well by the CMB data, where  $r_s$  and  $D_M$  are the comoving sound horizon and distance to the last scattering, respectively. We can understand the correlations between  $H_0$  and  $M_\nu$  and  $H_0$  and  $\xi_3$  in fitting the CMB data by a perturbative approach [32] (see Supplemental Materials for details). A small variation of  $M_\nu$  around a reference value  $M_\nu^{\text{ref}}$  would induce corresponding variations in  $r_s$  and  $D_M$ . We assume that  $H_0$  is varied accordingly so as to keep  $\theta_{\text{MC}}$  unchanged (fixed to the observed value). We therefore obtain,

$$C_H \frac{H_0 - H_0^{\text{ref}}}{H_0^{\text{ref}}} = C_m \frac{M_\nu - M_\nu^{\text{ref}}}{M_\nu^{\text{ref}}}, \quad (5)$$

where  $C_H$  and  $C_m$  can be calculated using the expressions for  $r_s$  and  $D_M$ . Similarly, we obtain the correlation between  $H_0$  and  $\xi_i$  by fixing  $M_\nu$  together with  $\theta_{\text{MC}}$  and

all other cosmological parameters:

$$C_H \frac{H_0 - H_0^{\text{ref}}}{H_0^{\text{ref}}} = \sum_i C_{\xi,i}^1 (\xi_i - \xi_i^{\text{ref}}) + \sum_i C_{\xi,i}^2 (\xi_i - \xi_i^{\text{ref}})^2. \quad (6)$$

The coefficients  $C_H, C_m, C_{\xi,i}^1, C_{\xi,i}^2$  are listed in Table III of Supplemental Materials. These semi-analytic results are shown in Figure 3, which agree well with the MCMC results. Moreover, we can obtain roughly the same 95% contours in the MCMC when the BAO data is included (see Supplemental Materials for details).

From the  $\Lambda\text{CDM}\xi_{\text{TT}}$  fitting results, we find a larger  $\Omega_b h^2$  ( $0.02325_{-0.00037}^{+0.00040}$ , 68% CL), compared with  $\Omega_b h^2 = 0.02242 \pm 0.00020$  from  $\Lambda\text{CDM}_{\text{TT}}$ . Based on this, we show in the Supplemental Materials that the BBN data also prefers  $\xi_3 = 1.22$ , which is consistent with our findings here.

#### scalar index $n_s$

The mean value of  $n_s$  in  $\Lambda\text{CDM}\xi_{\text{TT}}$  ( $n_s = 1.020_{-0.019}^{+0.020}$ , 68% CL) is consistent with 1 and  $3.1\sigma$  (MPCL) larger than that of  $\Lambda\text{CDM}_{\text{Planck}}$  ( $n_s = 0.9649 \pm 0.0042$ , 68% CL). This may have important implications on inflation models.

To quantify the implications of our results on inflation models, we vary one more parameter, the scalar-to-tensor ratio  $r$ , when fitting the TT data. The mean contours of  $n_s - r$  are shown in Figure 4. The brown curve shows one of the simplest hybrid models of [44], with the number of e-folds  $N$  between 50 and 60, where the energy density during inflation is dominated by the potential composed of two scalar fields  $\phi$  and  $\psi$ ,

$$V(\phi, \psi) = \frac{1}{4} \lambda (\psi^2 - M^2)^2 + \frac{1}{2} m^2 \phi^2 + \frac{1}{2} \lambda' \phi^2 \psi^2, \quad (7)$$

where we take  $\lambda = \lambda' = 1$  following [45] and fix the primordial perturbation amplitude  $A_s$  according to our CMB fitting results [44], so that we are left with only one parameter  $M$  (or  $m$ ). We obtain the upper bound for  $M$  ( $M_{\text{max}}$ ) (or  $m$  ( $m_{\text{max}}$ )) around  $1 \times 10^{-4} m_{\text{Pl}}$  ( $1 \times 10^{-8} m_{\text{Pl}}$ ), where  $m_{\text{Pl}} \equiv \sqrt{\hbar c/G}$  is the Planck mass. Moreover, other hybrid models, such as discussed in [44–46], can also be compatible with the results of  $\Lambda\text{CDM}\xi_{\text{TT}}$ . Furthermore, another kind of hybrid models, spontaneously broken supersymmetric (SB SUSY) theories [47], as shown in purple in Figure 4, is compatible with both  $\Lambda\text{CDM}_{\text{TT}}$  and  $\Lambda\text{CDM}\xi_{\text{TT}}$ . For all the above models, our results suggest a very small value of  $r$ . We also show monomial potential models  $V(\phi) \sim \phi^p$ , with  $p = 2, 1$  and  $2/3$  as red lines ( $50 < N < 60$ ) in Figure 4 for comparison [48–51].

	$M_\nu$ [eV]	$\xi_3$	$H_0$ [km s <sup>-1</sup> Mpc <sup>-1</sup> ]	$n_\sigma(H_0)$	$S_8$	$n_\sigma(S_8)$	$\ln K$
$\Lambda\text{CDM}_{\text{Planck}}$	0.06	0	$68.36 \pm 0.54$	4.9	$0.832 \pm 0.013$	2.8	—
$\Lambda\text{CDM}_{\text{TT}}$	0.06	0	$68.79 \pm 0.56$	3.6	$0.813 \pm 0.010$	2.2	-691.7
$\Lambda\text{CDM}_{\xi\text{TT}}$	$0.58^{+0.17}_{-0.13}$	$1.27^{+0.42}_{-0.22}$	$71.27^{+1.97}_{-2.04}$	0.8	$0.787 \pm 0.014$	1.1	-687.3

TABLE I. Mean values (68% CL) for  $M_\nu$ ,  $\xi_3$ ,  $H_0$  and  $S_8$  and their deviations (in unit of  $\sigma$ )  $n_\sigma$  with respect to the corresponding ‘tension’ measurements.  $\ln K$  is the Bayesian evidence.

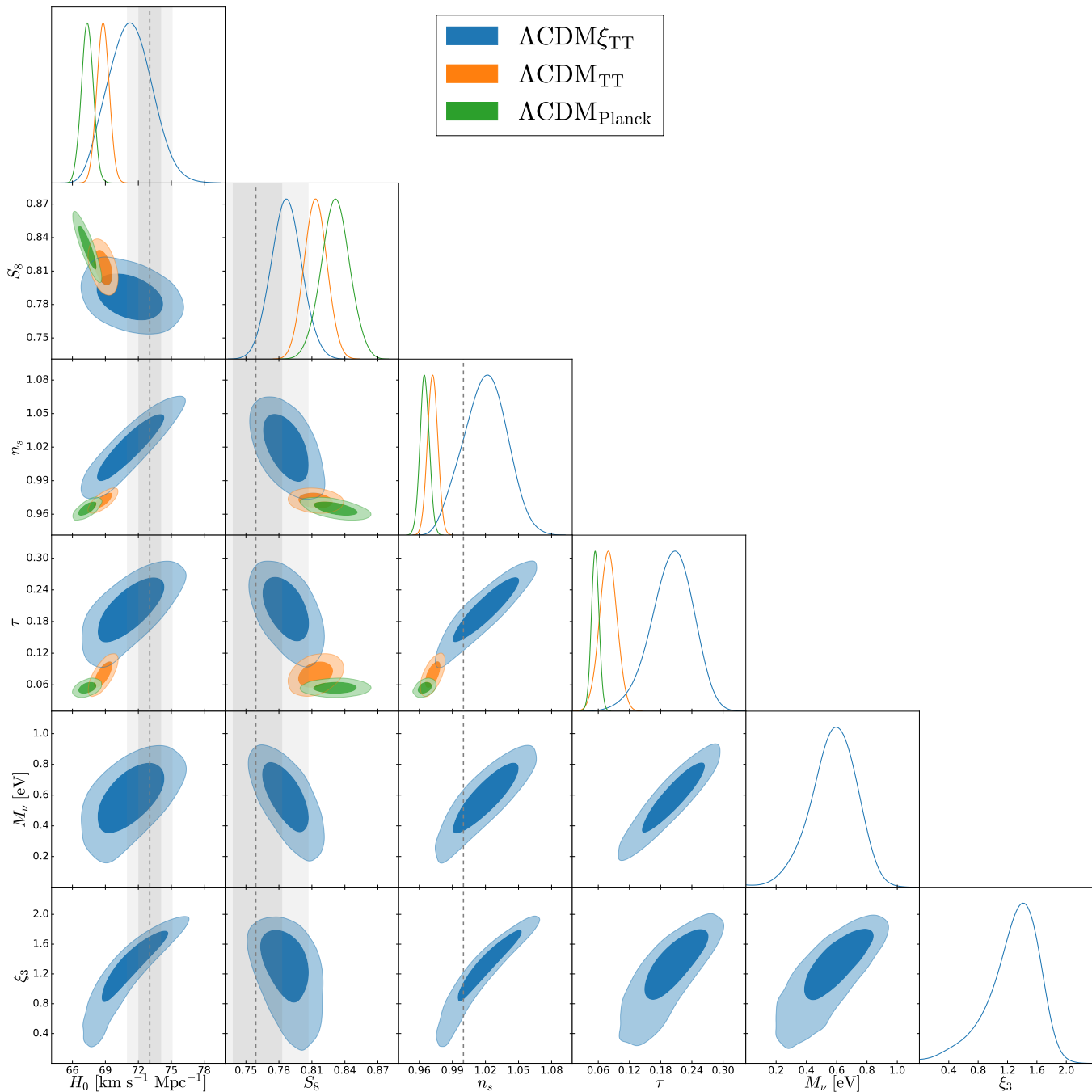


FIG. 2. Same as Figure 1, but for more selected cosmological and neutrino parameters, together with 1D marginalized posterior PDFs. The dashed line in panels for  $n_s$  indicates  $n_s = 1$ .

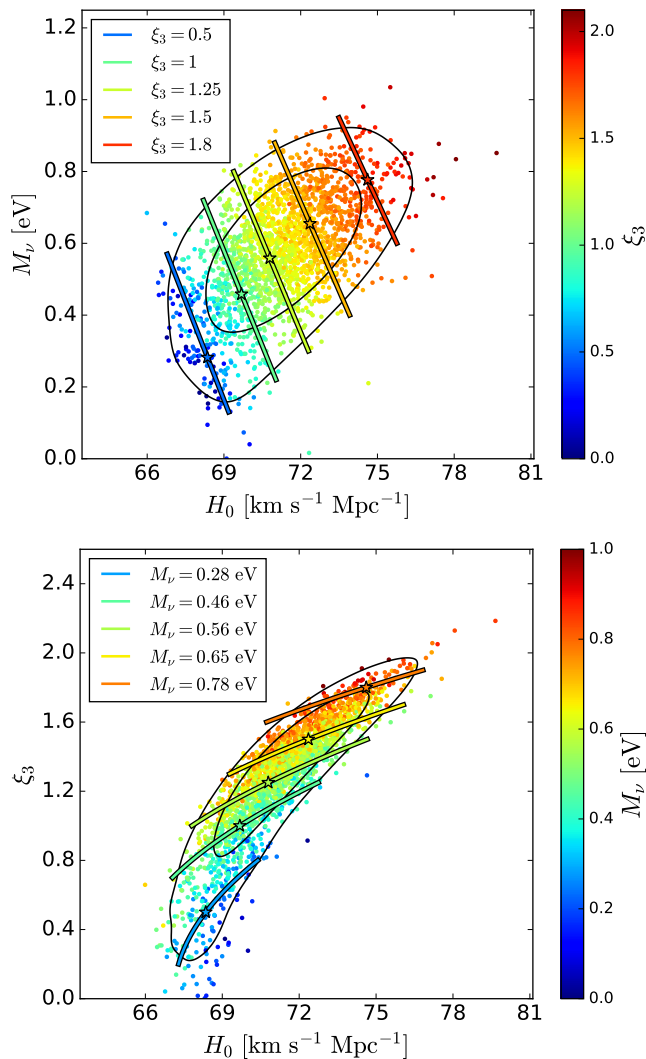


FIG. 3. PDFs for  $H_0$  and  $M_\nu$  ( $\xi_3$ ), with scatter points colored according to values of  $\xi_3$  ( $M_\nu$ ) in the top (bottom) panel. The colored lines are from Eqs. (5) and (6), with stars representing the corresponding reference points.

#### optical depth $\tau$

The mean value of the CMB optical depth from  $\Lambda\text{CDM}_{\xi\text{TT}}$  ( $\tau = 0.202^{+0.044}_{-0.036}$ ) is  $3.4\sigma$  (MPCL) larger than from  $\Lambda\text{CDM}_{\text{Planck}}$  ( $\tau = 0.0544 \pm 0.0073$ ). For  $\tau \approx 0.2$ , we can estimate the reionization redshift to be  $z \approx 20$  (see, e.g., Eq. (2) in [52]). This high reionization redshift may in fact be consistent with the recent JWST observation of high-redshift objects [53–57].

## CONCLUSION

In this letter, we fit *Planck* TT, lowT, plik–lensing, BAO and DES data with the  $\Lambda\text{CDM}$  and  $\Lambda\text{CDM}_\xi$  models. We find that the  $\Lambda\text{CDM}_\xi$  model is strongly preferred.

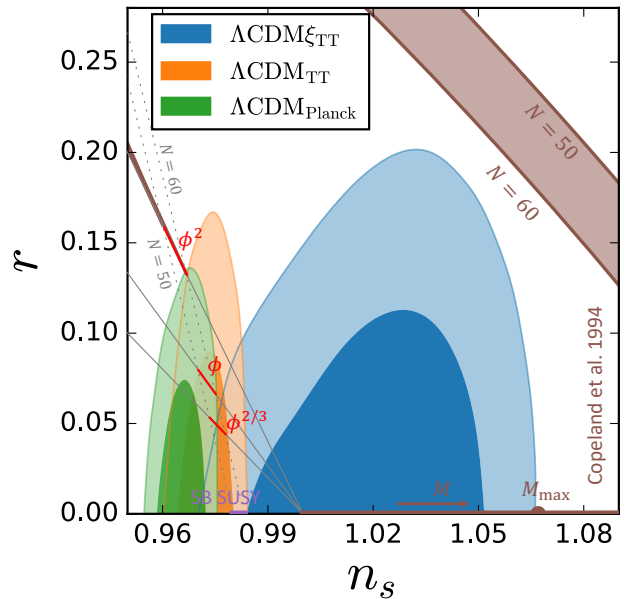


FIG. 4. Same as Figure 1 but for the  $n_s - r$  contours and several selected inflation models’ predictions, shown as red, purple and brown lines, with uncertainties in the number of e-folds of  $50 < N < 60$  (more details can be found in the main text).  $M_{\text{max}}$  is the upper bound of the model parameter  $M$  in [44].

Our main results are:

- (i) Both the  $H_0$  and  $S_8$  tensions are resolved with the same set of neutrino parameters. In particular, the global and local measurements of  $H_0$  and  $S_8$  agree to about  $1\sigma$ .
- (ii) There are around  $3\sigma$  evidences for both neutrino mass  $M_\nu = 0.58^{+0.17}_{-0.13}$  eV (68% CL) and degeneracy parameter  $\xi_3 = 1.27^{+0.42}_{-0.22}$  (68% CL), respectively. Moreover, this  $\mathcal{O}(1)$  neutrino degeneracy parameter is also consistent with the BBN data.
- (iii) The mean value of the scalar index  $n_s \gtrsim 1$  and is compatible with some hybrid inflation models.
- (iv) The mean value of the CMB optical depth  $\tau$  is much larger than the standard Planck result, suggesting an earlier onset of reionization, to  $z \approx 20$ .

Upcoming CMB observations, such as those from the South Pole Telescope (SPT-3G) [58], ACT [59], Simons Observatory [60], CMB-S4 [61, 62], the proposed CMB-HD [63–65], and other future missions could provide further tests of this  $\Lambda\text{CDM}_\xi$  model and more precise measurements of the neutrino parameters.

The computational resources used for the MCMCs in this work were kindly provided by the Chinese University of Hong Kong Central Research Computing Cluster. Furthermore, this research is supported by grants from the Research Grants Council of the Hong Kong Special Ad-

ministrative Region, China, under Project No. AoE/P-404/18 and 14300223. All plots in this paper are generated by `Getdist` [66] and `Matplotlib` [67], and we also use `Scipy` [68], and `Numpy` [69].

- 
- [1] Planck Collaboration, Planck 2018 results. VI. Cosmological parameters, *A&A* **641**, A6 (2020), arXiv:1807.06209 [astro-ph.CO].
- [2] S. Aiola et al., The Atacama Cosmology Telescope: DR4 maps and cosmological parameters, *J. Cosmology Astropart. Phys.* **2020**, 047 (2020), arXiv:2007.07288 [astro-ph.CO].
- [3] M. S. Madhavacheril et al., The Atacama Cosmology Telescope: DR6 Gravitational Lensing Map and Cosmological Parameters, arXiv e-prints, arXiv:2304.05203 (2023), arXiv:2304.05203 [astro-ph.CO].
- [4] H. du Mas des Bourboux et al., The Completed SDSS-IV Extended Baryon Oscillation Spectroscopic Survey: Baryon Acoustic Oscillations with Ly $\alpha$  Forests, *Astrophys. J.* **901**, 153 (2020), arXiv:2007.08995 [astro-ph.CO].
- [5] SPT-3G Collaboration, Constraints on  $\Lambda$  CDM extensions from the SPT-3G 2018 E E and T E power spectra, *Phys. Rev. D* **104**, 083509 (2021), arXiv:2103.13618 [astro-ph.CO].
- [6] SPT-3G Collaboration, Measurement of the CMB temperature power spectrum and constraints on cosmology from the SPT-3G 2018 T T, T E, and E E dataset, *Phys. Rev. D* **108**, 023510 (2023), arXiv:2212.05642 [astro-ph.CO].
- [7] DES Collaboration, Dark Energy Survey Year 3 results: Cosmological constraints from galaxy clustering and weak lensing, *Phys. Rev. D* **105**, 023520 (2022), arXiv:2105.13549 [astro-ph.CO].
- [8] A. G. Riess et al., A Comprehensive Measurement of the Local Value of the Hubble Constant with 1 km s $^{-1}$  Mpc $^{-1}$  Uncertainty from the Hubble Space Telescope and the SH0ES Team, *ApJ* **934**, L7 (2022), arXiv:2112.04510 [astro-ph.CO].
- [9] M. Asgari et al., KiDS-1000 cosmology: Cosmic shear constraints and comparison between two point statistics, *A&A* **645**, A104 (2021), arXiv:2007.15633 [astro-ph.CO].
- [10] D. Brout et al., The Pantheon+ Analysis: Cosmological Constraints, *Astrophys. J.* **938**, 110 (2022), arXiv:2202.04077 [astro-ph.CO].
- [11] R. Dalal et al., Hyper Suprime-Cam Year 3 results: Cosmology from cosmic shear power spectra, *Phys. Rev. D* **108**, 123519 (2023), arXiv:2304.00701 [astro-ph.CO].
- [12] X. Li et al., Hyper Suprime-Cam Year 3 results: Cosmology from cosmic shear two-point correlation functions, *Phys. Rev. D* **108**, 123518 (2023), arXiv:2304.00702 [astro-ph.CO].
- [13] S. More et al., Hyper Suprime-Cam Year 3 results: Measurements of clustering of SDSS-BOSS galaxies, galaxy-galaxy lensing, and cosmic shear, *Phys. Rev. D* **108**, 123520 (2023), arXiv:2304.00703 [astro-ph.CO].
- [14] S. Sugiyama et al., Hyper Suprime-Cam Year 3 results: Cosmology from galaxy clustering and weak lensing with HSC and SDSS using the minimal bias model, *Phys. Rev. D* **108**, 123521 (2023), arXiv:2304.00705 [astro-ph.CO].
- [15] H. Miyatake et al., Hyper Suprime-Cam Year 3 results: Cosmology from galaxy clustering and weak lensing with HSC and SDSS using the emulator based halo model, *Phys. Rev. D* **108**, 123517 (2023), arXiv:2304.00704 [astro-ph.CO].
- [16] E. Di Valentino et al., Nonminimal dark sector physics and cosmological tensions, *Phys. Rev. D* **101**, 063502 (2020), arXiv:1910.09853 [astro-ph.CO].
- [17] E. Di Valentino et al., Interacting dark energy in the early 2020s: A promising solution to the H $_0$  and cosmic shear tensions, *Physics of the Dark Universe* **30**, 100666 (2020), arXiv:1908.04281 [astro-ph.CO].
- [18] S. Kumar et al., Dark sector interaction: a remedy of the tensions between CMB and LSS data, *European Physical Journal C* **79**, 576 (2019), arXiv:1903.04865 [astro-ph.CO].
- [19] S. Kumar, Remedy of some cosmological tensions via effective phantom-like behavior of interacting vacuum energy, *Physics of the Dark Universe* **33**, 100862 (2021), arXiv:2102.12902 [astro-ph.CO].
- [20] Z. Berezhiani et al., Reconciling Planck results with low redshift astronomical measurements, *Phys. Rev. D* **92**, 061303 (2015), arXiv:1505.03644 [astro-ph.CO].
- [21] J. Solà Peracaula et al., Running vacuum against the H $_0$  and  $\sigma_8$  tensions, *EPL (Europhysics Letters)* **134**, 19001 (2021).
- [22] Ö. Akarsu et al., Relaxing cosmological tensions with a sign switching cosmological constant, *Phys. Rev. D* **104**, 123512 (2021), arXiv:2108.09239 [astro-ph.CO].
- [23] Ö. Akarsu et al., Relaxing cosmological tensions with a sign switching cosmological constant: Improved results with Planck, BAO, and Pantheon data, *Phys. Rev. D* **108**, 023513 (2023), arXiv:2211.05742 [astro-ph.CO].
- [24] S.-F. Yan et al., Interpreting cosmological tensions from the effective field theory of torsional gravity, *Phys. Rev. D* **101**, 121301 (2020), arXiv:1909.06388 [astro-ph.CO].
- [25] E. Abdalla et al., Cosmology intertwined: A review of the particle physics, astrophysics, and cosmology associated with the cosmological tensions and anomalies, *Journal of High Energy Astrophysics* **34**, 49 (2022), arXiv:2203.06142 [astro-ph.CO].
- [26] E. Di Valentino et al., In the realm of the Hubble tension—a review of solutions, *Classical and Quantum Gravity* **38**, 153001 (2021), arXiv:2103.01183 [astro-ph.CO].
- [27] N. Schöneberg et al., The H $_0$  Olympics: A fair ranking of proposed models, *Phys. Rep.* **984**, 1 (2022), arXiv:2107.10291 [astro-ph.CO].
- [28] A. Rida Khalife et al., Review of Hubble tension solutions with new SH0ES and SPT-3G data, arXiv e-prints, arXiv:2312.09814 (2023), arXiv:2312.09814 [astro-ph.CO].
- [29] A.-K. Burns et al., Indications for a Nonzero Lepton Asymmetry from Extremely Metal-Poor Galaxies, *Phys. Rev. Lett.* **130**, 131001 (2023), arXiv:2206.00693 [hep-ph].
- [30] M. Escudero et al., Primordial lepton asymmetries in the precision cosmology era: Current status and future sensitivities from BBN and the CMB, *Phys. Rev. D* **107**, 035024 (2023), arXiv:2208.03201 [hep-ph].
- [31] G. Barenboim et al., Flavor versus mass eigenstates in neutrino asymmetries: implications for cosmology, *European Physical Journal C* **77**, 590 (2017), arXiv:1609.03200 [astro-ph.CO].

- [32] S. Yeung et al., Relic neutrino degeneracies and their impact on cosmological parameters, *J. Cosmology Astropart. Phys.* **2021**, 024 (2021), arXiv:2010.01696 [astro-ph.CO].
- [33] F. Beutler et al., The 6dF Galaxy Survey: baryon acoustic oscillations and the local Hubble constant, *MNRAS* **416**, 3017 (2011), arXiv:1106.3366 [astro-ph.CO].
- [34] A. J. Ross et al., The clustering of the SDSS DR7 main Galaxy sample - I. A 4 per cent distance measure at  $z = 0.15$ , *MNRAS* **449**, 835 (2015), arXiv:1409.3242 [astro-ph.CO].
- [35] S. Alam et al., The clustering of galaxies in the completed SDSS-III Baryon Oscillation Spectroscopic Survey: cosmological analysis of the DR12 galaxy sample, *MNRAS* **470**, 2617 (2017), arXiv:1607.03155 [astro-ph.CO].
- [36] Dark Energy Survey Collaboration, Dark Energy Survey year 1 results: Cosmological constraints from galaxy clustering and weak lensing, *Phys. Rev. D* **98**, 043526 (2018), arXiv:1708.01530 [astro-ph.CO].
- [37] G. Barenboim et al., Flavor versus mass eigenstates in neutrino asymmetries: implications for cosmology, *European Physical Journal C* **77**, 590 (2017), arXiv:1609.03200 [astro-ph.CO].
- [38] A. Lewis et al., Efficient Computation of Cosmic Microwave Background Anisotropies in Closed Friedmann-Robertson-Walker Models, *Astrophys. J.* **538**, 473 (2000), arXiv:astro-ph/9911177 [astro-ph].
- [39] A. Lewis et al., *cmbant/CAMB: 1.0.12* (2019).
- [40] W. Giarè et al., Measuring the reionization optical depth without large-scale CMB polarization, *arXiv e-prints*, arXiv:2312.06482 (2023), arXiv:2312.06482 [astro-ph.CO].
- [41] A. Lewis and S. Bridle, Cosmological parameters from CMB and other data: A Monte Carlo approach, *Phys. Rev. D* **66**, 103511 (2002), arXiv:astro-ph/0205436 [astro-ph].
- [42] A. Lewis et al., *cmbant/CosmoMC: October 2019* (2019).
- [43] A. Heavens et al., Marginal Likelihoods from Monte Carlo Markov Chains, *arXiv e-prints*, arXiv:1704.03472 (2017), arXiv:1704.03472 [stat.CO].
- [44] E. J. Copeland et al., False vacuum inflation with Einstein gravity, *Phys. Rev. D* **49**, 6410 (1994), arXiv:astro-ph/9401011 [astro-ph].
- [45] M. Cortès and A. R. Liddle, Viable inflationary models ending with a first-order phase transition, *Phys. Rev. D* **80**, 083524 (2009), arXiv:0905.0289 [astro-ph.CO].
- [46] A. Linde, Hybrid inflation, *Phys. Rev. D* **49**, 748 (1994), arXiv:astro-ph/9307002 [astro-ph].
- [47] G. Dvali et al., Large scale structure and supersymmetric inflation without fine tuning, *Phys. Rev. Lett.* **73**, 1886 (1994), arXiv:hep-ph/9406319 [hep-ph].
- [48] A. D. Linde, Chaotic inflation, *Physics Letters B* **129**, 177 (1983).
- [49] E. Silverstein and A. Westphal, Monodromy in the CMB: Gravity waves and string inflation, *Phys. Rev. D* **78**, 106003 (2008), arXiv:0803.3085 [hep-th].
- [50] L. McAllister et al., Gravity waves and linear inflation from axion monodromy, *Phys. Rev. D* **82**, 046003 (2010), arXiv:0808.0706 [hep-th].
- [51] L. McAllister et al., The powers of monodromy, *Journal of High Energy Physics* **2014**, 123 (2014), arXiv:1405.3652 [hep-th].
- [52] R. de Belsunce et al., Inference of the optical depth to reionization from low multipole temperature and polarization Planck data, *MNRAS* **507**, 1072 (2021), arXiv:2103.14378 [astro-ph.CO].
- [53] I. Labbé et al., A population of red candidate massive galaxies 600 Myr after the Big Bang, *Nature (London)* **616**, 266 (2023), arXiv:2207.12446 [astro-ph.GA].
- [54] Y. Harikane et al., A Comprehensive Study of Galaxies at  $z = 9-16$  Found in the Early JWST Data: Ultraviolet Luminosity Functions and Cosmic Star Formation History at the Pre-reionization Epoch, *ApJS* **265**, 5 (2023), arXiv:2208.01612 [astro-ph.GA].
- [55] M. Castellano et al., Early Results from GLASS-JWST. III. Galaxy Candidates at  $z = 9-15$ , *ApJ* **938**, L15 (2022), arXiv:2207.09436 [astro-ph.GA].
- [56] R. P. Naidu et al., Two Remarkably Luminous Galaxy Candidates at  $z \approx 10-12$  Revealed by JWST, *ApJ* **940**, L14 (2022), arXiv:2207.09434 [astro-ph.GA].
- [57] H. Yan et al., First Batch of  $z \approx 11-20$  Candidate Objects Revealed by the James Webb Space Telescope Early Release Observations on SMACS 0723-73, *ApJ* **942**, L9 (2023), arXiv:2207.11558 [astro-ph.GA].
- [58] B. A. Benson et al., SPT-3G: a next-generation cosmic microwave background polarization experiment on the South Pole telescope, in *Millimeter, Submillimeter, and Far-Infrared Detectors and Instrumentation for Astronomy VII*, Society of Photo-Optical Instrumentation Engineers (SPIE) Conference Series, Vol. 9153, edited by W. S. Holland and J. Zmuidzinas (2014) p. 91531P, arXiv:1407.2973 [astro-ph.IM].
- [59] S. W. Henderson et al., Advanced ACTPol Cryogenic Detector Arrays and Readout, *Journal of Low Temperature Physics* **184**, 772 (2016), arXiv:1510.02809 [astro-ph.IM].
- [60] Simons Observatory Collaboration, The Simons Observatory: science goals and forecasts, *J. Cosmology Astropart. Phys.* **2019**, 056 (2019), arXiv:1808.07445 [astro-ph.CO].
- [61] K. N. Abazajian et al., CMB-S4 Science Book, First Edition, *arXiv e-prints*, arXiv:1610.02743 (2016), arXiv:1610.02743 [astro-ph.CO].
- [62] K. Abazajian et al., CMB-S4 Science Case, Reference Design, and Project Plan, *arXiv e-prints*, arXiv:1907.04473 (2019), arXiv:1907.04473 [astro-ph.IM].
- [63] N. Sehgal et al., CMB-HD: An Ultra-Deep, High-Resolution Millimeter-Wave Survey Over Half the Sky, in *Bulletin of the American Astronomical Society*, Vol. 51 (2019) p. 6, arXiv:1906.10134 [astro-ph.CO].
- [64] N. Sehgal et al., Science from an Ultra-Deep, High-Resolution Millimeter-Wave Survey, *BAAS* **51**, 43 (2019), arXiv:1903.03263 [astro-ph.CO].
- [65] N. Sehgal et al., CMB-HD: Astro2020 RFI Response, *arXiv e-prints*, arXiv:2002.12714 (2020), arXiv:2002.12714 [astro-ph.CO].
- [66] A. Lewis, GetDist: a Python package for analysing Monte Carlo samples, *arXiv e-prints*, arXiv:1910.13970 (2019), arXiv:1910.13970 [astro-ph.IM].
- [67] J. D. Hunter, Matplotlib: A 2D Graphics Environment, *Computing in Science and Engineering* **9**, 90 (2007).
- [68] SciPy 1.0 Contributors, SciPy 1.0: fundamental algorithms for scientific computing in Python, *Nature Methods* **17**, 261 (2020), arXiv:1907.10121 [cs.MS].
- [69] C. R. Harris et al., Array programming with NumPy, *Nature (London)* **585**, 357 (2020), arXiv:2006.10256 [cs.MS].
- [70] Planck Collaboration, Planck 2013 results. XVI. Cosmological parameters, *A&A* **571**, A16 (2014),

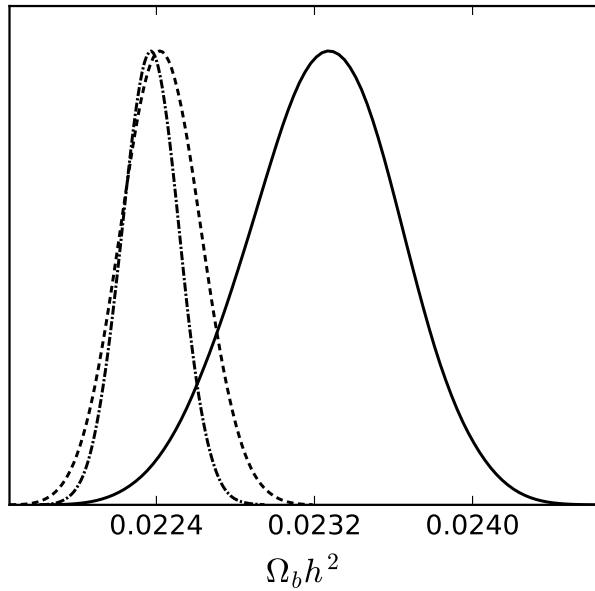


FIG. 5. Posterior distribution of baryon density  $\Omega_b h^2$  obtained from  $\Lambda\text{CDM}_{\text{Planck}}$  (dash-dotted),  $\Lambda\text{CDM}_{\text{TT}}$  (dashed), and  $\Lambda\text{CDM}_{\xi\text{TT}}$  (solid).

arXiv:1303.5076 [astro-ph.CO].

[71] C. Pitrou et al., Precision big bang nucleosynthesis with improved Helium-4 predictions, *Phys. Rep.* **754**, 1 (2018), arXiv:1801.08023 [astro-ph.CO].

## SUPPLEMENTAL MATERIALS

### Full parameter table

Table II shows all cosmological parameters with 68% CL from  $\Lambda\text{CDM}_{\text{Planck}}$ ,  $\Lambda\text{CDM}_{\text{TT}}$ , and  $\Lambda\text{CDM}_{\xi\text{TT}}$ , and we follow the definitions of the cosmological parameters as shown in Table 1 of [70]. The first group shows the free parameters used in each case, while the second group denotes the derived parameters based on the first group.

### Consistency with BBN

As shown in Figure 5 or Table II, for the cosmological baryon density, we obtain  $\Omega_b h^2 = 0.02325^{+0.00040}_{-0.00037}$  68% C.L. from  $\Lambda\text{CDM}_{\xi\text{TT}}$ . Our result is significantly larger than that from  $\Lambda\text{CDM}_{\text{TT}}$  ( $\Omega_b h^2 = 0.02242 \pm 0.00020$ ).

To estimate the implication of a larger  $\Omega_b h^2$  on BBN, we adopt the following fitting formulae [71],

$$\begin{aligned} \frac{\Delta Y_p}{\bar{Y}_p} &= 0.04 \frac{\Delta \Omega_b h^2}{\Omega_b h^2} + 0.16 \frac{\Delta N_\nu}{3.0} - 0.96 \xi_{\nu_e}, \\ \frac{\Delta D/H}{\bar{D}/H} &= -1.65 \frac{\Delta \Omega_b h^2}{\Omega_b h^2} + 0.41 \frac{\Delta N_\nu}{3.0} - 0.53 \xi_{\nu_e}. \end{aligned} \quad (8)$$

The bars over the symbols represent the corresponding reference values used in [71]. To keep the measured quantities of BBN unchanged, i.e., the LHS of Eq. (8) equals zero, but the baryon density  $\Omega_b h^2$  changes from the reference value 0.02225 to 0.02325 (i.e.,  $\overline{\Omega_b h^2} = 0.02225$  and  $\Delta \Omega_b h^2 = 0.02325 - 0.02225$ ), we obtain  $\Delta N_\nu = 0.71$  and  $\xi_{\nu_e} = 0.04$ . During the BBN period, neutrinos are relativistic particles, so we have

$$\Delta N_\nu = \frac{15}{7} \sum_i \left( \frac{\xi_i}{\pi} \right)^2 \left[ 2 + \left( \frac{\xi_i}{\pi} \right)^2 \right]. \quad (9)$$

We thus obtain

$$\begin{aligned} \xi_1 &= -0.05, \\ \xi_2 &= 0.14, \\ \xi_3 &= 1.22. \end{aligned} \quad (10)$$

This result is consistent with our results in the main text.

## Semi-analytic model on $H_0$

### Perturbation analysis of $\theta_{\text{MC}}$

In this section, following [32], we use a semi-analytic approach to understand the neutrino effects on  $H_0$ . We start from the sound horizon angular size ( $\theta_{\text{MC}}$ ) at the epoch of photon decoupling  $z_*$ ,

$$\theta_{\text{MC}} = \frac{r_s}{D_M}, \quad (11)$$

where  $r_s$  and  $D_M$  are the comoving sound horizon and distance to the last scattering, respectively,

$$\begin{aligned} r_s(z_*) &= \int_{z_*}^{\infty} \frac{dz}{\sqrt{3(1+R)H(z)}}, \\ D_M(z_*) &= \int_0^{z_*} \frac{dz}{H(z)}, \end{aligned} \quad (12)$$

where  $R \equiv 3\rho_b/4\rho_\gamma$  is the ratio between baryon and photon energy densities.

For convenience, we take  $c = \hbar = k_B = 1$  and define the following kernels

$$\begin{aligned} G(x, \xi_i) &\equiv \frac{1}{e^{x-\xi_i} + 1} + \frac{1}{e^{x+\xi_i} + 1}, \\ F(x, \xi_i) &\equiv \frac{1}{e^{x-\xi_i} + 1} - \frac{1}{e^{x+\xi_i} + 1}, \\ K_1(x, y) &= 2x\sqrt{x^2 + y^2} + \frac{x^3}{\sqrt{x^2 + y^2}}, \\ K_2(x, y) &= 2\sqrt{x^2 + y^2} + \frac{5x^2}{\sqrt{x^2 + y^2}} - \frac{x^4}{(x^2 + y^2)^{3/2}}, \end{aligned} \quad (13)$$



Parameter	$\Lambda\text{CDM}_{\text{Planck}}$	$\Lambda\text{CDM}_{\text{TT}}$	$\Lambda\text{CDM}_{\xi\text{TT}}$
$\Omega_b h^2$	$0.02237 \pm 0.00015$	$0.02242 \pm 0.00020$	$0.02325_{-0.00037}^{+0.00040}$
$\Omega_c h^2$	$0.1200 \pm 0.0012$	$0.1166 \pm 0.0012$	$0.1225_{-0.0048}^{+0.0046}$
$100\theta_{\text{MC}}$	$1.04092 \pm 0.00031$	$1.04119 \pm 0.00042$	$1.04056 \pm 0.00058$
$\tau$	$0.0544 \pm 0.0073$	$0.079_{-0.016}^{+0.017}$	$0.202_{-0.036}^{+0.044}$
$\ln(10^{10} A_s)$	$3.044 \pm 0.014$	$3.085_{-0.030}^{+0.031}$	$3.339_{-0.075}^{+0.092}$
$n_s$	$0.9649 \pm 0.0042$	$0.9721 \pm 0.0046$	$1.020_{-0.019}^{+0.021}$
$M_\nu$	—	—	$0.58_{-0.13}^{+0.17}$
$\xi_3$	—	—	$1.27_{-0.22}^{+0.42}$
$H_0[\text{km s}^{-1} \text{Mpc}^{-1}]$	$67.36 \pm 0.54$	$68.79 \pm 0.56$	$71.3 \pm 2.0$
$\Omega_\Lambda$	$0.6847 \pm 0.0073$	$0.7048 \pm 0.0069$	$0.6976 \pm 0.0085$
$\Omega_m$	$0.3153 \pm 0.0073$	$0.2952 \pm 0.0069$	$0.3024 \pm 0.0085$
$\Omega_m h^2$	$0.1430 \pm 0.0011$	$0.1396 \pm 0.0011$	$0.1536_{-0.0074}^{+0.0071}$
$\Omega_m h^3$	$0.09633 \pm 0.00030$	$0.09605_{-0.00046}^{+0.00045}$	$0.1096_{-0.0085}^{+0.0074}$
$\sigma_8$	$0.8111 \pm 0.0060$	$0.820 \pm 0.010$	$0.784 \pm 0.017$
$S_8 \equiv \sigma_8(\Omega_m/0.3)^{0.5}$	$0.832 \pm 0.013$	$0.813 \pm 0.010$	$0.787 \pm 0.014$
$\sigma_8 \Omega_m^{0.25}$	$0.6078 \pm 0.0064$	$0.6044 \pm 0.0069$	$0.581 \pm 0.011$
$z_{re}$	$7.67 \pm 0.73$	$9.9_{-1.3}^{+1.5}$	$19.4_{-2.4}^{+3.2}$
$10^9 A_s$	$2.100 \pm 0.030$	$2.187_{-0.066}^{+0.067}$	$2.83 \pm 0.24$
$10^9 A_s e^{-2\tau}$	$1.883 \pm 0.011$	$1.866 \pm 0.011$	$1.882 \pm 0.018$
Age[Gyr]	$13.797 \pm 0.023$	$13.764 \pm 0.029$	$13.21_{-0.34}^{+0.32}$
$z_*$	$1089.92 \pm 0.25$	$1089.55 \pm 0.30$	$1090.0_{-0.60}^{+0.50}$
$r_*[\text{Mpc}]$	$144.43 \pm 0.26$	$145.29 \pm 0.30$	$139.0_{-3.5}^{+3.2}$
$100\theta_*$	$1.04110 \pm 0.00031$	$1.04139 \pm 0.00041$	$1.04044_{-0.00078}^{+0.00072}$
$z_{\text{drag}}$	$1059.94 \pm 0.30$	$1059.81 \pm 0.45$	$1062.9_{-1.4}^{+1.5}$
$r_{\text{drag}}[\text{Mpc}]$	$147.09 \pm 0.26$	$147.96 \pm 0.33$	$141.3_{-3.7}^{+3.4}$
$k_{\text{D}}[\text{Mpc}^{-1}]$	$0.14087 \pm 0.00030$	$0.13999 \pm 0.00042$	$0.1449_{-0.0028}^{+0.0027}$
$z_{\text{eq}}$	$3402 \pm 26$	$3321 \pm 27$	$3482_{-123}^{+117}$
$k_{\text{eq}}[\text{Mpc}^{-1}]$	$0.010384 \pm 0.000081$	$0.010137_{-0.000082}^{+0.000083}$	$0.01095_{-0.00055}^{+0.00052}$
$100\theta_{s,\text{eq}}$	$0.4594 \pm 0.0026$	$0.4572 \pm 0.0027$	$0.439_{-0.013}^{+0.012}$

TABLE II. Mean values of cosmological parameters (68% CL) for  $\Lambda\text{CDM}_{\text{Planck}}$ ,  $\Lambda\text{CDM}_{\text{TT}}$  and  $\Lambda\text{CDM}_{\xi\text{TT}}$ . The first group lists free parameters used in each case, while the second group shows the derived parameters based on the first group.

and functionals

$$\mathcal{I}_r[f(z)] \equiv \int_{z_*}^{\infty} \frac{f(z)}{[H^{\text{ref}}(z)]^3} \frac{dz}{\sqrt{3(1+R)}}, \quad (14)$$

$$\mathcal{I}_D[f(z)] \equiv \int_0^{z_*} \frac{f(z)}{[H^{\text{ref}}(z)]^3} dz.$$

As  $\theta_{\text{MC}}$  is well constrained by CMB data, we expand  $r_s$  and  $D_M$  around reference values of  $M_\nu$  and  $H_0$ , denoted as  $M_\nu^{\text{ref}}$  and  $H_0^{\text{ref}}$ , to the lowest order by fixing  $\theta_{\text{MC}}$ ,  $\xi_i$  and other cosmological parameters ( $\Omega_b h^2, \Omega_c h^2, \Omega_\gamma h^2$ ). We get,

$$C_H \frac{H_0 - H_0^{\text{ref}}}{H_0^{\text{ref}}} = C_m \frac{M_\nu - M_\nu^{\text{ref}}}{M_\nu^{\text{ref}}}, \quad (15)$$

where

$$\begin{aligned} C_H &= \mathcal{I}_r(1) - \theta_{\text{MC}} \mathcal{I}_D(1), \\ C_m &= \theta_{\text{MC}} \mathcal{I}_D[C_{\rho m}(z) - (1+z)^3 C_{\rho m}(0)] \\ &\quad - \mathcal{I}_r[C_{\rho m}(z) - (1+z)^3 C_{\rho m}(0)], \end{aligned} \quad (16)$$

$$C_{\rho m}(z) = \frac{T_{\nu 0}^4 (1+z)^2}{4\pi^2 \rho_{\text{crit},0}^{\text{ref}}} \int_0^\infty dx \sum_i G(x, \xi_i) \frac{x^2 \tilde{m}_i^2}{\sqrt{x^2 + (\tilde{m}_i/(1+z))^2}}, \quad (17)$$

and  $\tilde{m}_i \equiv m_i/T_{\nu 0}$ .  $T_{\nu 0}$  and  $\rho_{\text{crit},0}$  are the relic neutrino temperature and critical energy density of the Universe today, respectively.

Similarly, we expand around  $\xi_i^{\text{ref}}$  ( $i = 1, 2, 3$ ) and  $H_0^{\text{ref}}$  to investigate the correlation between  $\xi_i$  and  $H_0$ , while for  $\xi_i$ , we keep up to the second order term,

$$C_H \frac{H_0 - H_0^{\text{ref}}}{H_0^{\text{ref}}} = \sum_i C_{\xi,i}^1 (\xi_i - \xi_i^{\text{ref}}) + \sum_i C_{\xi,i}^2 (\xi_i - \xi_i^{\text{ref}})^2, \quad (18)$$

where

$$\begin{aligned} C_{\xi,i}^1 &= \theta_{\text{MC}} \mathcal{I}_D[C_{\rho \xi,i}^1(z) - (1+z)^3 C_{\rho \xi,i}^1(0)] \\ &\quad - \mathcal{I}_r[C_{\rho \xi,i}^1(z) - (1+z)^3 C_{\rho \xi,i}^1(0)], \\ C_{\xi,i}^2 &= \theta_{\text{MC}} \mathcal{I}_D[C_{\rho \xi,i}^2(z) - (1+z)^3 C_{\rho \xi,i}^2(0)] \\ &\quad - \mathcal{I}_r[C_{\rho \xi,i}^2(z) - (1+z)^3 C_{\rho \xi,i}^2(0)], \end{aligned} \quad (19)$$

$\xi_3^{\text{ref}}$	0.5	1	1.25	1.5	1.8
$M_\nu^{\text{ref}}$ [eV]	0.28	0.46	0.56	0.65	0.78
$H_0^{\text{ref}}$ [km s <sup>-1</sup> Mpc <sup>-1</sup> ]	68.4	69.7	70.8	72.4	74.6
$C_m/C_H$	-0.023	-0.037	-0.046	-0.055	-0.067
$C_{\xi,1}^1/C_H$	-0.005	-0.010	-0.012	-0.015	-0.018
$C_{\xi,2}^1/C_H$	0.006	0.011	0.014	0.017	0.021
$C_{\xi,3}^1/C_H$	0.075	0.151	0.191	0.231	0.279
$C_{\xi,1}^2/C_H$	0.073	0.069	0.066	0.062	0.058
$C_{\xi,2}^2/C_H$	0.073	0.069	0.066	0.063	0.058
$C_{\xi,3}^2/C_H$	0.078	0.090	0.098	0.106	0.117

TABLE III. Selected expansion reference points and calculated coefficients of Eqs. (16) and (19).

$$C_{\rho\xi,i}^1(z) = \frac{T_{\nu 0}^4(1+z)^4}{4\pi^2\rho_{\text{crit},0}^{\text{ref}}} \int_0^\infty dx K_1(x, \tilde{m}_i/(1+z)) F(x, \xi_i),$$

$$C_{\rho\xi,i}^2(z) = \frac{T_{\nu 0}^4(1+z)^4}{8\pi^2\rho_{\text{crit},0}^{\text{ref}}} \int_0^\infty dx K_2(x, \tilde{m}_i/(1+z)) G(x, \xi_i). \quad (20)$$

We can find from above that, when  $\xi_i$  approaches zero,  $F(x, \xi_i) \rightarrow 0$ , then  $C_{\rho\xi,i}^1$  also approaches zero, causing the first-order coefficient ( $C_{\xi,i}^1$ ) to become negligible and allowing the second-order perturbation term to dominate. Conversely, when  $\xi_i \sim \mathcal{O}(1)$ , the first-order term takes precedence. Therefore, unlike  $M_\nu$ , it is necessary to terms up to second order in  $\xi_i$ .

We choose five  $\xi_3^{\text{ref}}$  points, and obtain the corresponding  $M_\nu^{\text{ref}}$  and  $H_0^{\text{ref}}$  from the mean values in MCMC chains with fixing  $\xi_3^{\text{ref}}$ . The reference values for  $\xi_3^{\text{ref}}$ ,  $M_\nu^{\text{ref}}$  and  $H_0^{\text{ref}}$  are listed in Table III. Then, the corresponding coefficients ( $C_m/C_H$ ,  $C_{\xi,i}^1/C_H$  and  $C_{\xi,i}^2/C_H$ ) can be calculated according to Eqs. (16) and (19), which are also summarized in Table III.

From Figure 3 in the main text, we find that our perturbation analyses agree well with the MCMC results.

### BAO constraints

Based on the derived relation between  $(M_\nu, H_0)$  or  $(\xi_3, H_0)$ , we can estimate the constraints from BAO data. Here, we use BAO data in [33–35], as summarized in Table IV, where  $r_{\text{drag}}$  is the comoving sound horizon at

$z_{\text{drag}}$ ,

$$r_{\text{drag}} = \int_{z_{\text{drag}}}^\infty \frac{dz}{\sqrt{3(1+R)H(z)}}, \quad (21)$$

and

$$D_V(z) \equiv \left[ D_M^2(z) \frac{z}{H(z)} \right]^{1/3}. \quad (22)$$

We define the quantities used in [35] as  $\mathbf{d}$ ,

$$\mathbf{d} \equiv \left( r_{d,\text{fid}} \frac{D_M(z_1)}{r_{\text{drag}}}, H(z_1) \frac{r_{\text{drag}}}{r_{d,\text{fid}}}, r_{d,\text{fid}} \frac{D_M(z_2)}{r_{\text{drag}}}, H(z_2) \frac{r_{\text{drag}}}{r_{d,\text{fid}}}, r_{d,\text{fid}} \frac{D_M(z_3)}{r_{\text{drag}}}, H(z_3) \frac{r_{\text{drag}}}{r_{d,\text{fid}}} \right). \quad (23)$$

Then we define  $\chi^2$  as

$$\chi^2 = \sum_{ij} \mathbf{d}_i C_{ij}^{-1} \mathbf{d}_j^T + \left[ \frac{r_{\text{drag}}/D_V(z_4) - 0.336}{0.015} \right]^2 + \left[ \frac{r_{\text{drag}}/D_V(z_5) - 4.46}{0.17} \right]^2, \quad (24)$$

where  $C_{ij}$  is the covariance matrix between the BAO measurements [35]

$$C_{ij} = \begin{pmatrix} 624.707 & 23.729 & 325.332 & 8.34963 & 157.386 & 3.57778 \\ 23.729 & 5.60873 & 11.6429 & 2.33996 & 6.39263 & 0.968056 \\ 325.332 & 11.6429 & 905.777 & 29.3392 & 515.271 & 14.1013 \\ 8.34963 & 2.33996 & 29.3392 & 5.42327 & 16.1422 & 2.85334 \\ 157.386 & 6.39263 & 515.271 & 16.1422 & 1375.12 & 40.4327 \\ 3.57778 & 0.968056 & 14.1013 & 2.85334 & 40.4327 & 6.25936 \end{pmatrix}. \quad (25)$$

Then, we can compute the likelihood function

$$\mathcal{L} \sim e^{-\chi^2/2}, \quad (26)$$

based on BAO observations and determine the  $2\sigma$  range of  $\mathcal{L}$ , as shown in the left two panels in Figure 6. The results for  $(M_\nu, H_0)$  and  $(\xi_3, H_0)$  are shown in the upper and lower right panels of Figure 6, respectively. This estimation roughly aligns with the 95% contours in the MCMC results.

$z$	$z_1$	$z_2$	$z_3$	$z_4$	$z_5$
	0.38	0.51	0.61	0.106	0.15
$r_{d,\text{fid}}D_M(z)/r_{\text{drag}}(z)$ [Mpc]	1512.39	1975.22	2306.68	–	–
$H(z)r_{\text{drag}}(z)/r_{d,\text{fid}}$ [ $\text{km s}^{-1} \text{Mpc}^{-1}$ ]	81.2087	90.9029	98.9647	–	–
$r_{\text{drag}}(z)/D_V(z)$	–	–	–	$0.336 \pm 0.015$	–
$D_V(z)/r_{\text{drag}}(z)$	–	–	–	–	$4.46 \pm 0.17$

TABLE IV. BAO measurements at various redshifts. The first group is from [35] with fiducial  $r_{d,\text{fid}} = 147.78$  Mpc, while the subsequent datasets are obtained from [33] and [34], respectively.

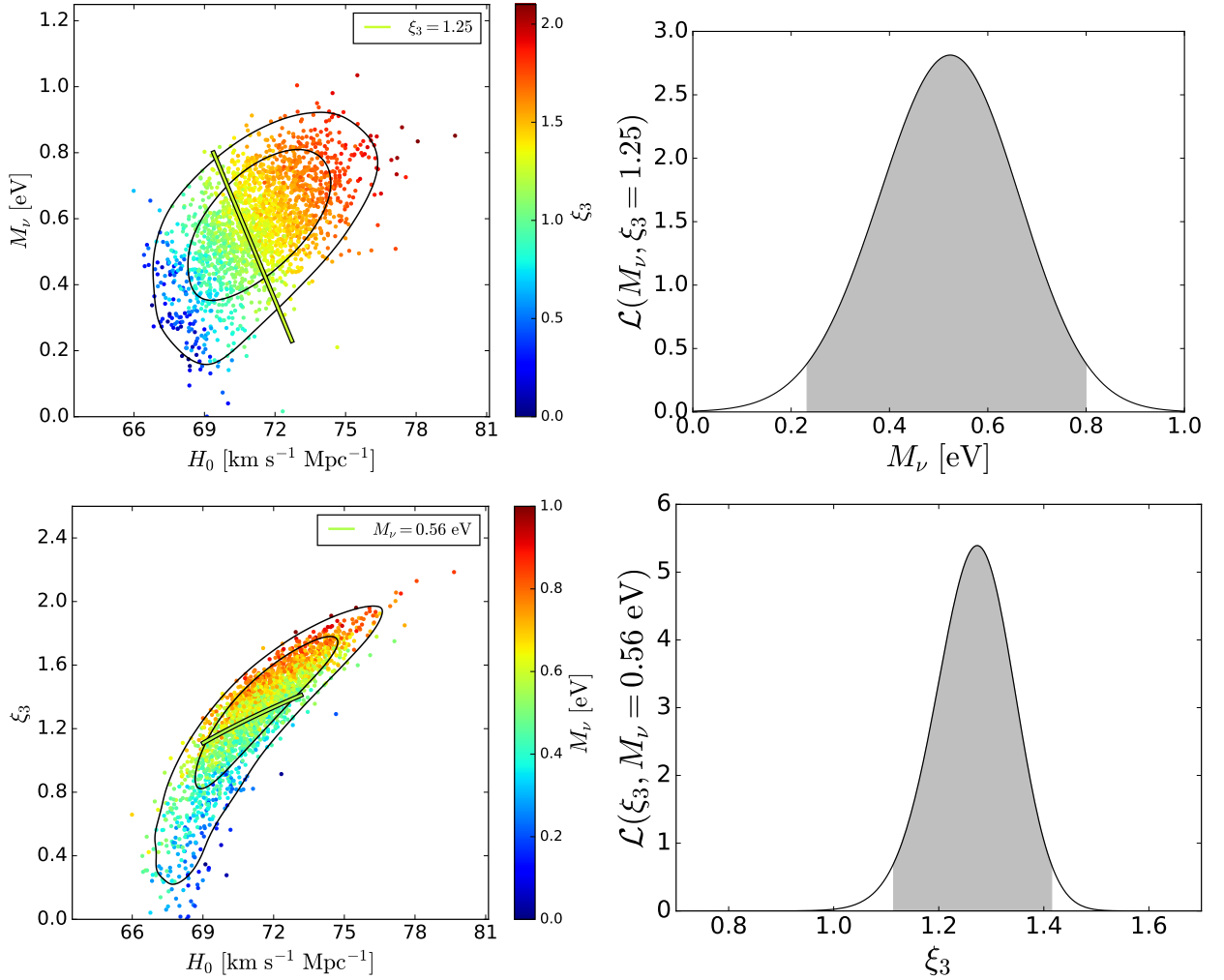


FIG. 6. Left panels are the same as Figure 3 in the main text, but with the the yellow lines constrained by BAO data. The right panels show the corresponding normalized likelihood  $\mathcal{L}$ , with the shaded areas representing 95% CL.